ACS Catalysis

Research Article

pubs.acs.org/acscatalysis

Structure and Reactivity of Zn-Modified ZSM-5 Zeolites: The Importance of Clustered Cationic Zn Complexes

Sami M. T. Almutairi, Brahim Mezari, Pieter C. M. M. Magusin, Evgeny A. Pidko,* and Emiel J. M. Hensen

Inorganic Materials Chemistry, Eindhoven University of Technology, P.O. Box 513, 5600 MB Eindhoven, The Netherlands

Supporting Information

ABSTRACT: A novel route for the introduction of well-defined zinc species into ZSM-5 zeolite via chemical vapor deposition of dimethylzinc (CVD(DMZ)) is explored. The structural properties and catalytic reactivity of the synthesized material (Zn/ZSM-5-CVD(DMZ)) are investigated against a set of Zn/ZSM-5 catalysts prepared by incipient wetness impregnation (IWI), ion exchange (IE), and high-temperature reaction with zinc vapor (CVD(m)). The materials are characterized by a range of physicochemical methods including temperature programmed reduction (TPR), in situ FTIR, magic-angle spinning (MAS) NMR, and X-ray absorption spectroscopy (XAS). The catalysts are tested for their activity in the dehydrogenation of propane. Catalysts prepared by IE and IWI exhibit a high degree of heterogeneity of extraframework zinc species. These include, besides isolated Zn^{2+} cations, multinuclear oxygenated zinc clusters and bulk zinc oxide aggregates. The CVD(m) method results in quantitative replacement of all Brønsted acid protons by isolated Zn^{2+}. In CVD(DMZ) the Brønsted acid sites (BAS) react stoichiometrically with dimethylzinc $Zn(CH_3)_2$ (DMZ) yielding grafted $[Zn\text{-}CH_3]^+$ species, which can further be transformed to isolated Zn^{2+} ions by reduction in hydrogen. The presence of zinc in ZSM-5 enhances the rate of alkane dehydrogenation. The initial activity of Zn/ZSM-5 prepared by IWI and IE correlates with the Zn content. The samples with a more heterogeneous distribution of extraframework Zn species are more active than the samples with isolated Zn^{2+}. The activity of reduced Zn/ZSM-5-CVD(DMZ) containing predominantly isolated Zn^{2+} ions can be substantially increased by oxidation prior to the reaction. However, the resulting oxygenated complexes easily decompose during the reaction. Propane dehydrogenation and catalyst stability of Zn/ZSM-5-CVD(DMZ) can be improved by addition of steam to the hydrocarbon feed. This rate enhancement is ascribed to an increase of the steady-state concentration of the reactive oxygenated sites.

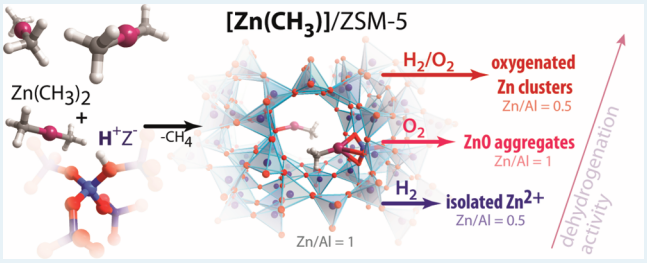

KEYWORDS: *Zn/ZSM-5, zeolite, alkane dehydrogenation, chemical vapor deposition, dimethylzinc, X-ray absorption spectroscopy, in situ FTIR, MAS NMR, oxygenated zinc clusters*

1. INTRODUCTION

High-silica ZSM-5 zeolites modified with zinc (Zn/ZSM-5) are active catalysts for the dehydrogenation and aromatization of light alkanes.[1−4] The reaction mechanism involves a complex set of steps including dehydrogenation, oligomerization, and ring-closure reactions. The modifying zinc cations play a key role in the dehydrogenation of paraffins, whereas the Brønsted acid sites (BAS) of the zeolite are responsible for the oligomerization and aromatization of the resulting olefins. Many experimental[3−9] and theoretical[10−22] studies have been devoted to the nature of the active sites and the mechanism of propane activation by zinc-exchanged high-silica zeolites, but the exact nature and role of the different zinc species is still under debate.[2−22]

The zinc speciation depends on the topology and Si/Al ratio of the zeolite, as well as the method of Zn introduction including the overall Zn content and subsequent thermochemical activation.[23] Zinc-containing ZSM-5 can be prepared by incipient wetness impregnation (IWI), ion exchange (IE) in aqueous solution, and chemical vapor deposition (CVD) techniques. When conventional techniques such as IWI or IE are employed, Zn/ZSM-5 will contain (i) isolated Zn^{2+} ions stabilized at the cation-exchange sites of the zeolite, (ii) binuclear $[ZnOZn]^{2+}$ clusters resulting from the condensation of partially hydrolyzed $ZnOH^+$ extraframework cations, and (iii) more bulky intrazeolite or extrazeolite clusters of zinc oxide. Broadly speaking, IWI results in higher Zn content than IE with a more homogeneous speciation typical for the latter case.[4,3,6,24] Although it is usually assumed that only isolated extraframework Zn^{2+} cations are formed during IE, the formation of binuclear $[ZnOZn]^{2+}$ complexes has also been demonstrated for overexchanged zeolite samples.[25] An alternative and completely anhydrous method for the introduction of Zn into zeolite matrixes is based on the chemical reaction between zinc vapor and the BAS of the

Received: August 26, 2011
Revised: December 2, 2011
Published: December 5, 2011

zeolite. This technique results in a quantitative replacement of all zeolitic BAS by isolated Zn^{2+} cations.[26−30]

The nature of the catalytically active Zn sites in Zn/ZSM-5 is still a matter of dispute. It has been demonstrated that the catalytic reactivity[2,31] and adsorption[27,32] properties of both impregnated and ion-exchanged zeolites with relatively low Zn/Al ratios are similar to those of the catalysts prepared by a high-temperature reaction with zinc vapor. Besides other evidence,[4] these observations led to the conclusion that the active sites in Zn/ZSM-5 for alkane dehydrogenation are isolated Zn^{2+} ions. In contrast, recent in situ NMR studies by Stepanov et al.[33−38] point to a key role of multinuclear Zn_nO_m aggregates for the catalytic reactivity of overexchanged zeolites. The direct experimental comparison of the catalytic reactivity of Zn/ZSM-5 catalysts containing predominantly one of the above active sites has not been achieved yet.

A theoretical approach to the identification of the active site has also been taken in recent years.[39,40] The initial heterolytic CH activation over the bare Zn^{2+} involves the formation of zinc alkyl surface species and a zeolitic BAS, whereas alkane activation over the oxygenated zinc clusters leads to the formation of extraframework zinc alkyl species and ZnOH groups. Both mechanisms have so far been supported by experimental spectroscopic studies.[27,29,30,32−38,41,42] The heterolytic dissociation of alkanes over isolated Zn^{2+} has been evidenced by in situ DRIFTS[27,32] and MAS NMR[29,30] spectroscopies for Zn/ZSM-5 materials prepared by a high-temperature reaction of HZSM-5 with Zn^0 (Zn/Al = 0.15−0.5). The crucial role of ZnO aggregates confined in the pores of zeolites ZSM-5 and BEA for alkane activation has been demonstrated in a series of in situ MAS NMR studies by Stepanov et al.[33−38] and in combined in situ MAS NMR and IR spectroscopic studies by Ivanova et al.[41,42] involving Zn-modified materials with a Zn content in excesss of the IE capacity of the parent zeolites (Zn/Al > 1).

Theoretical calculations show that the initial CH activation by oxygenated Zn complexes is more favorable because of the higher basicity of the extraframework O ligands compared to the lattice oxygens of the zeolite and therefore their higher affinity toward H^+.[39] The subsequent closure of the catalytic cycle by H_2 recombination and regeneration of the initial catalytic site is much more difficult for the binuclear Zn complexes. Therefore, it has been concluded that isolated Zn^{2+} cations are the preferred active sites for the dehydrogenation of alkanes.

Until now only CVD of metallic zinc was employed for the preparation of well-defined Zn-zeolite samples. However, in this way only a *single* type of extraframework Zn species, namely, isolated Zn^{2+} cations, can be introduced. An alternative method makes use of the surface organometallic chemistry approach. In our previous studies, we have demonstrated that a wide range of well-defined Ga species can be selectively introduced into high-silica ZSM-5 zeolite by CVD of $Ga(CH_3)_3$ followed by specific thermochemical activation.[43−46] By using the volatile precursor dimethylzinc $Zn(CH_3)_2$ (DMZ) such a synthetic route can, in principle, also be followed to obtain well-defined Zn/ZSM-5. Previously, CVD of DMZ has been used as a selective analytical tool for the titration of OH groups on various solids such as silica, alumina, and molecular sieves.[47−53] Already at room temperature DMZ reacts with surface hydroxyls resulting in grafted $Zn(CH_3)^+$ species and methane. There are only a few examples of the use of DMZ for the modification of zeolites. Zn-modified SAPO materials were prepared by DMZ CVD to improve their reactivity in the conversion of oxygenated hydrocarbons to olefins.[52] The CVD of DMZ on ZSM-5 zeolite followed by steaming was proposed to improve the conversion of alkanes to aromatics and lower olefins.[54]

Herein, we explore the possibility to prepare Zn-modified ZSM-5 via selective reaction of HZSM-5 with DMZ. The influence of the postsynthetic treatment on the nature and reactivity of Zn/ZSM-5 is investigated. The state of Zn in the resulting Zn/ZSM-5 is studied by using a range of physicochemical methods including temperature programmed reduction (TPR), Fourier transform infrared spectroscopy (FTIR), and X-ray absorption spectroscopy (XAS). The results for the DMZ-modified Zn/ZSM-5 are interpreted on the basis of the data obtained for samples prepared by more conventional techniques such as IWI, IE, and high-temperature reaction with zinc vapor. All zeolitic materials are tested for their activity in the propane dehydroaromatization.

2. EXPERIMENTAL SECTION

2.1. Catalyst Preparation. Ammonium forms of two ZSM-5 zeolites with Si/Al ratios of 20 and 40 (kindly provided by Albemarle Catalysts) were calcined in a mixture of 20 vol % oxygen in nitrogen at a flow rate of 100 N mL/min while heating to 550 °C at a heating rate of 2°/min followed by an isothermal period of 6 h to obtain the hydrogen forms of the zeolites. These zeolites are denoted by HZSM-5(20) and HZSM-5(40). Zinc was introduced following various methods including IWI, IE, and CVD to yield Zn/ZSM-5 zeolites. The resulting zeolite catalysts are designated in the following manner: Zn/ZSM-5(x)-*M*-(y), where x is the Si/Al ratio in the parent zeolite, *M* stands for the preparation method (IWI, IE, or CVD) and y refers to the Zn/Al ratio. For the Zn/ZSM-5 zeolites prepared by CVD methods, CVD(m) and CVD(DMZ) notations are used to distinguish the high-temperature CVD of zinc vapor (m) and the low temperature reaction with the organometallic precursor dimethylzinc (DMZ).

Zn/ZSM-5(x)-IWI-(y) samples were prepared by impregnating the proton form of the parent zeolites previously dehydrated at 120 °C for 16 h with aqueous solutions of $Zn(OAc)_2{\cdot}2H_2O$ (98+%, Sigma-Aldrich) . The impregnation procedure was followed by drying at 120 °C for 16 h and calcination at 550 °C (heating rate of 2°/min) in a mixture of 20 vol % oxygen in nitrogen for 4 h.

For IE, the parent HZSM-5(x) zeolites were contacted with an aqueous solution of 0.005 M $Zn(NO_3)_2{\cdot}H_2O$ (>99.0%, Merck) at 70 °C for 1, 4, and 16 h. Subsequently, the zeolites were washed with distilled water, dried at 120 °C for 16 h, and calcined at 550 °C in the artificial air for 4 h. In this case, the catalysts are denoted by Zn/ZSM-5(x)-IE(z h)-(y) catalysts, where z indicates the duration of the IE procedure in h.

Zn/ZSM-5(20)-CVD(m) catalyst was prepared by the chemical reaction of dehydrated HZSM-5(20) with zinc vapor at 550 °C under dynamic vacuum. The resulting material was kept in a nitrogen-flushed glovebox.

Zn/ZSM-5(20)-CVD(DMZ) was prepared by CVD of $Zn(CH_3)_2$ (dimethylzinc, DMZ, ABCR Chemicals, 95%) on dehydrated HZSM-5(20). All manipulations were performed in a nitrogen-flushed glovebox. To a glass vessel containing dehydrated HZSM-5 (20), 1 mL of DMZ was added. After 24 h, the resulting material was evacuated for 2 h to remove unreacted dimethylzinc and reaction products. The resulting material was kept in a nitrogen-flushed glovebox. Before the

dx.doi.org/10.1021/cs200441e | ACS Catal. 2012, 2, 71−83

catalytic tests, the CVD(DMZ) samples were either calcined in a 20% O_2/N_2 mixture or reduced in pure H_2 for 2 h at 550 °C resulting in, respectively, Zn/ZSM-5(20)-CVD(DMZ)/OX and Zn/ZSM-5(20)-CVD(DMZ)/RED samples.

2.2. Catalyst Characterization. *X-ray Diffraction (XRD).* The integrity of the zeolite structure following the different preparation methods was followed by X-ray diffraction (XRD). XRD patterns were recorded on a Bruker D4 Endeavor Diffractometer using CuKα radiation with a wavelength of 1.54056 Å. 2θ angles from 5° to 60° were measured with a step size of 0.077° and a time per step of 1 s. The catalysts were ground and pressed in sample holders for measurements.

Nitrogen Physisorption. Nitrogen sorption measurements were performed using a Micromeritics TriStar 3000 apparatus. Prior to measuring the isotherm, the zeolite sample(~100 mg) was outgassed at 150 °C for 3 h and cooled to liquid N_2 temperature.

Elemental Analysis. Zn and Al contents in the synthesized materials were determined by elemental analysis that was carried out by ICP-OES (Spectro Ciros CCD ICP optical emission spectrometer with axial plasma viewing). For the ICP measurements the catalysts were dissolved in a 1.5 mL solution of $HF/HNO_3/H_2O$ (1:1:1) acid mixture.

Temperature Programmed Reduction (TPR). TPR measurements were carried out in a flow apparatus using two TCD detectors. An amount of sample was placed in a quartz tube between two quartz wool plugs and introduced in an oven. Prior to reduction, the sample was calcined at 450 °C (10 °C/min) in 5% O_2 in He for 1 h. Then, the sample was cooled to room temperature in N_2 flow. The TPR measurements were performed in a flow of 5 vol % H_2 in N_2 under heating at a ramp of 10 °C/min until a temperature of 800 °C was reached. For the samples prepared by CVD the TPR measurement was performed with the as-prepared samples without the prior oxidation in O_2/N_2 (contact with air was avoided by sealing the quartz tubes with plastic plugs after introducing the sample in the glovebox). The hydrogen signal was calibrated by using a CuO/SiO_2 reference material with known Cu content.

Fourier Transform Infrared Spectroscopy (FTIR). FTIR spectra were recorded with a Bruker Vertex V70 FTIR spectrometer in transmission mode. Typically, about 10 mg zeolite sample was pressed into a self-supporting wafer (diameter 13 mm) and placed in a controlled-environment transmission cell. The spectra were normalized to the thickness of the wafer, determined from the weight of the sample in the dehydrated state. Prior to recording spectra, the zeolites were dehydrated in an O_2 flow while heating from room temperature to 550 °C at a heating rate of 5 °C/min. After an isothermal period of 1 h at 550 °C, the sample was evacuated for 50 min at 550 °C and cooled to room temperature in vacuum.

The reaction of DMZ with Brønsted acid sites of the zeolite and the subsequent conversion of the grafted organozinc species was monitored by FTIR spectroscopy. To this end, an amount of HZSM-5(20) sample was placed in the cell, dehydrated, and evacuated followed by short exposure to DMZ vapor at room temperature. After a hold time of 20 min, the sample was evacuated for 2 h and subsequently either reduced (H_2) or oxidized (O_2) at a pressure of 50 mbar and increasing temperatures (100, 200, 300, 400, and 500 °C) for 30 min followed by evacuation at each temperature setting and recording an FTIR spectrum. For comparison similar experiments were performed with pure SiO_2.

Solid-State NMR. For NMR characterization a fresh Zn/ZSM-5-CVD(DMZ) sample was prepared by adding a drop of DMZ to a small amount of dehydrated HZSM-5(20) at room temperature in a nitrogen-flushed glovebox. Before packing a small portion of Zn/ZSM-5-CVD(DMZ) into the NMR sample holder, it was given a few minutes time to release methane resulting from the reaction and unreacted DMZ. Another sample for NMR measurements was prepared by transferring the remainder in a static reactor and exposure to H_2 at 300 °C.

^{1}H and ^{13}C MAS NMR spectra were recorded on a Bruker DMX500 spectrometer operating at ^{1}H and ^{13}C NMR frequencies of 500 and 125 MHz, respectively. The spectrometer was equipped with a 2.5-mm MAS NMR probehead, and the samples were rotated in dry nitrogen at rate of 25 kHz for ^{1}H NMR and 8 kHz for ^{13}C NMR. Direct-excitation ^{1}H and ^{13}C NMR were obtained by use of a Hahn-echo pulse sequence (HEPS) 90°-τ-180°-τ with a 90°-pulse duration of 5 μs and two short delays τ of 2.5 μs to suppress baseline artifacts from pulse leakage and background signals from the probehead. For ^{13}C NMR signal enhancement also ^{1}H−^{13}C cross-polarization was used with a (shaped) contact pulse of 5 ms. The interscan delay was 20 s for direct excitation ^{1}H and ^{13}C NMR, and 5 s for ^{1}H−^{13}C cross-polarization NMR. ^{1}H-{^{27}Al} TRAPDOR[55,56] spectra were recorded with a HEPS with delays τ equal to 0.75 ms and ^{27}Al NMR irradiation during the time interval τ after the 180° pulse in the pulse sequence. Estimated from the 180° pulse on a $Al(NO_3)_3$ solution, the ^{27}Al nutation frequency was 50 kHz.

XAS at the Zn K-Edge. XAS measurements were measured in a controlled atmosphere transmission cell. Catalyst samples were pressed in self-supporting pellets with an optimal thickness adjusted to have an absorption μx of about 2.5. Spectra were recorded at the Zn K edge in transmission mode. The experiments were performed at the DUBBLE beamline at the ESRF, Grenoble, France (storage ring 6.0 GeV, ring current 200 mA). The EXAFS oscillation $\chi(E)$ in energy space was extracted from the experimentally measured absorption coefficient $\mu(E)$ by subtracting an isolated atom-like background absorption function $\mu_0(E)$ using $\chi(E) = (\mu(E) - \mu_0(E))/\mu_0(E)$. $\chi(E)$ was then converted into k-space $\chi(k)$ with $k = 2\pi(2m_e(E - E_0)/h^2)^{1/2}$, where m_e is the electron mass. Structural information was extracted from the k^3-weighted EXAFS function by multiple shell fitting in R-space until a satisfactory fit was obtained by k^1 and k^3 weighting. EXAFS analysis was performed with EXCURVE on k^3-weighted unfiltered raw data using the curved wave theory. Phase shifts were derived from ab initio calculations using Hedin−Lundqvist exchange potentials and Von Barth ground states. Energy calibration was carried out with Zn foil. The estimated accuracies of the EXAFS fit parameters were ±20% for the coordination number (N), ± 0.04 Å for the coordination distance (R), ± 20% for the Debye−Waller factor $\Delta\sigma^2$ and ±10% for the inner-potential correction ΔE_0.

2.3. Catalytic Activity Measurements. The zeolite catalysts were tested for their activity in propane aromatization in an atmospheric-pressure single-pass quartz microflow reactor at 550 °C. The feed mixture was delivered by thermal mass flow controllers and consisted of 5 vol % C_3H_8 in He (Linde gas) at a total flow rate of 100 mL/min. The WHSV space velocity was kept at 11.7 h^{-1}. The product composition was analyzed by an online three-column gas chromatograph (Compact GC,

dx.doi.org/10.1021/cs200441e | ACS Catal. 2012, 2, 71−83

Table 1. Elemental Analysis and Physicochemical Properties of Zn/ZSM-5 Catalysts[a]

samples	Si/Al	Zn/Al	Zn loading, wt %	BET surface area, m^2/g	pore volume, mL/g	crystallinty, %
HZSM-5(20)	20	0	0	375	0.19	100
HZSM-5(40)	40	0	0	411	0.26	100
Zn/ZSM-5(20)-IWI-(0.09)	20	0.09	0.45	341	0.19	96
Zn/ZSM-5(20)-IWI-(0.16)	20	0.16	0.82	325	0.18	95
Zn/ZSM-5(20)-IWI-(0.40)	20	0.40	2	306	0.17	98
Zn/ZSM-5(20)-IWI-(0.70)	20	0.70	3.5	155	0.1	92
Zn/ZSM-5(40)-IWI-(0.11)	40	0.11	0.31	399	0.25	95
Zn/ZSM-5(40)-IWI-(0.26)	40	0.26	0.69	393	0.25	98
Zn/ZSM-5(40)-IWI-(0.38)	40	0.38	1	387	0.24	96
Zn/ZSM-5(40)-IWI-(1.01)	40	1.01	2.6	337	0.23	92
Zn/ZSM-5(20)-IE(1 h)-(0.07)	20	0.07	0.35	359	0.2	94
Zn/ZSM-5(20)-IE(4 h)-(0.10)	20	0.1	0.5	299	0.18	93
Zn/ZSM-5(20)-IE(16 h)-(0.17)	20	0.17	0.9	177	0.11	91
Zn/ZSM-5(40)-IE(1 h)-(0.11)	40	0.11	0.31	329	0.19	98
Zn/ZSM-5(40)-IE(4 h)-(0.15)	40	0.15	0.4	293	0.18	96
Zn/ZSM-5(40)-IE(16 h)-(0.29)	40	0.29	0.78	290	0.18	96
Zn/ZSM-5(20)-CVD(m)-(0.57)	20	0.57	2.9	n.d.	n.d.	n.d.
Zn/ZSM-5(20)-CVD(DMZ)-(1.06)	20	1.06	5.3	n.d.	n.d.	n.d.
Zn/ZSM-5(20)-CVD(DMZ)/RED-(0.41)	20	0.41	2.1	n.d.	n.d.	n.d.
Zn/ZSM-5(20)-CVD(DMZ)/OX-(1.00)	20	1.00	4.9	n.d.	n.d.	n.d.

[a]n.d. = not determined. BET = Brunauer−Emmett−Teller .

Interscience) equipped with a PLOT Al_2O_3/KCl column with a flame ionization detector and Molsieve-5 Å and RTX-1 columns both employing termal conductivity detectors.

3. RESULTS AND DISCUSSION

3.1. Synthesis of Materials. The main results of the physicochemical characterization of Zn/ZSM-5 zeolites are summarized in Table 1. The method by which Zn is introduced has a strong influence on the final Zn loading, but not on the crystallinity and textural properties of the calcined zeolites. Typically, the surface area and pore volume decrease upon introduction of Zn and the changes are more pronounced with higher Zn content.

When the catalysts were prepared by IWI, the Zn loading was controlled by the Zn^{2+} concentration in the impregnation solution. For both HZSM-5(20) and HZSM-5(40) four catalysts with different Zn content were prepared. In each series, two samples are under-exchanged, that is, the Zn/Al ratio is lower than 0.5 (Zn/ZSM-5(20)-IWI-(0.09), Zn/ZSM-5(20)-IWI-(0.16), Zn/ZSM-5(40)-IWI-(0.11), and Zn/ZSM-5(40)-IWI-(0.26)). The Zn content of Zn/ZSM-5(20)-IWI-(0.40) and Zn/ZSM-5(40)-IWI-(0.38) is close to the theoretical exchange capacity for bivalent cations. Zn/ZSM-5(20)-IWI-(0.70) and Zn/ZSM-5(40)-IWI-(1.01) have Zn/Al ratios in excess of 0.5 and correspond therefore to the so-called overexchanged.

For the IE samples, the maximum zinc loading was ∼0.9 wt % (Zn/Al = 0.17) for HZSM-5(20) = 20 and ∼0.78 wt % (Zn/Al = 0.29) for HZSM-5(40). The major fraction of zinc is introduced at the early stages of IE. A short 1 h exchange already leads to the exchange of 14 and 22% of zeolitic cationic sites with Zn^{2+} for HZSM-5(20) and HZSM-5(40), respectively. After IE for 4 h, the exchange level increased only slightly, whereas IE for 16 h yields zeolites with 34 and 58% exchange levels for Si/Al = 20 and 40, respectively. Surprisingly, in spite of the lower overall Al content and thus expected lower concentration of paired Al sites for HZSM-5(40), slightly higher exchange levels were achieved for this zeolite. This indicates either a different Al distribution in the two materials or a more extensive formation of partially hydrolyzed, monovalent $[Zn{-}OH]^+$ species in Zn/ZSM-5(40)-IE.

The composition of the two Zn/ZSM-5 materials prepared by CVD was quite different. High temperature CVD of Zn vapor led to a Zn/Al ratio of 0.57 (Zn/HZSM-5(20)-CVD(m)-(0.57)), which is close to the earlier reported value of 0.5.[32] The reaction involves oxidation of Zn^0 by zeolitic BAS resulting in Zn^{2+} ions according to

$$Zn^0 + 2H^+Z^- \rightarrow Z^-Zn^{2+}Z^- + H_2 \quad (1)$$

,where H^+Z^- denotes zeolitic BAS and Z^- stands for the anionic framework site of the zeolite.

Since only a limited fraction of the oxygen-occupied aluminum tetrahedra are arranged in a pairwise manner that can stabilize Zn^{2+} by direct charge compensation, it is concluded that part of the charge compensation is indirect, that is, the divalent Zn cation is located at one exchange site with the another one left unoccupied. The excess Zn loading compared to the theoretical value of 0.50 is likely due to the presence of residual Zn^0 in the catalyst sample.

The Zn content is much higher (Zn/Al = 1.06) when the CVD is carried out with DMZ at room temperature (Zn/ZSM-5(20)-CVD(DMZ)-(1.06)). The introduction of Zn in this case involves the reaction

$$Zn(CH_3)_2 + H^+Z^- \rightarrow [Zn(CH_3)]^+Z^- + CH_4 \quad (2)$$

.

This reaction proceeds stoichiometrically with respect to the number of BAS and, accordingly, the Al content (more than 95% of the aluminum atoms in both parent ZSM-5 samples are part of the framework as determined by ^{27}Al NMR). The excess in this case results from the reaction of silanol groups at the external zeolite surface with DMZ. Subsequent high-temperature treatment of Zn/ZSM-5(20)-CVD(DMZ)-(1.06) in H_2 results in a decrease of the Zn/Al ratio to 0.41 (Zn/ZSM-5(20)-CVD/RED-(0.41)). The loss of Zn is caused by the

dx.doi.org/10.1021/cs200441e | ACS Catal. 2012, 2, 71−83

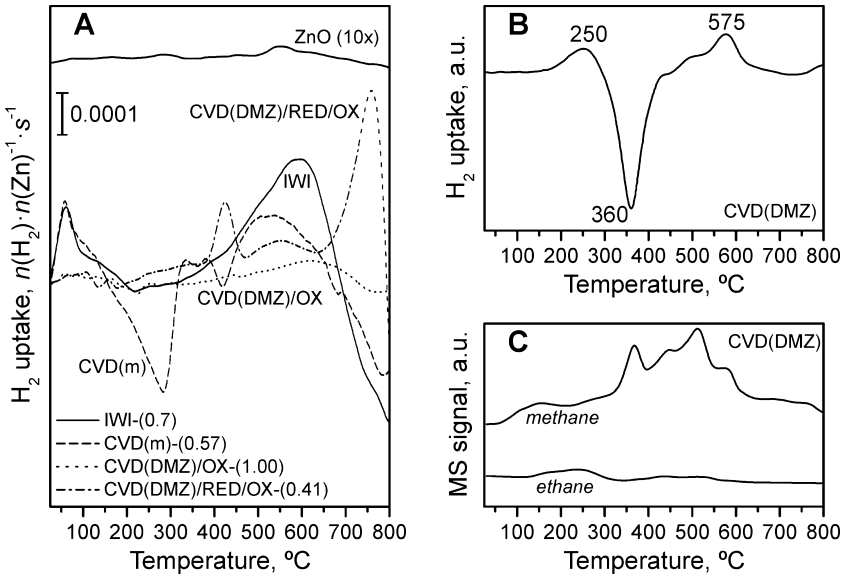

Figure 1. Temperature programmed reduction (TPR) profiles of (A) selected Zn/ZSM-5(20)-IWI, Zn/ZSM-5(20)-IE, and Zn/ZSM-5(20)-CVD(m), and oxygenated Zn/ZSM-5(20)-CVD(DMZ)/OX and Zn/ZSM-5(20)-CVD(DMZ)/RED/OX samples as well as ZnO reference material. (B) TPR profile of Zn/ZSM-5(20)-CVD(DMZ) zeolite and (C) the associated evolution of methane and ethane.

reduction of the grafted Zn-methyl complexes according to

$$2[Zn(CH_3)]^+Z^- + H_2 \rightarrow Z^-Zn^{2+}Z^- + Zn^0 + 2CH_4 \quad (3)$$

,with the metallic Zn evaporating as evidenced by the formation of a reflecting Zn coating on the cold part of the quartz reactor tube.

Alternatively, the grafted Zn-methyl complexes can be decomposed by high-temperature oxidation in O_2. The resulting Zn/ZSM-5(20)-CVD/OX-(1.00) catalyst has a similar Zn content as the precursor. We tentatively propose that the reaction in this case proceeds according to

$$n[Zn(CH_3)]^+Z^- + O_2 \rightarrow Zn_nO_m{}^{n+}(Z^-)_n + CO_2 + H_2O \quad (4)$$

.A partial hydrolysis of the intrazeolitic zinc complexes by water formed because of the oxidation of the methyl ligands cannot be excluded in this case.

3.2. Temperature Programmed Reduction. TPR profiles for the pure ZnO reference sample and a selection of Zn/ZSM-5 samples are shown in Figure 1 A. The quantitative data derived from these experiments are summarized in Table 2. For

Table 2. Summary of TPR Results for ZnZSM-5(20)-IWI and Oxygenated Zn/ZSM-5(20)-CVD(DMZ) Materials

		reduction temperature (°C)			
sample	Zn (wt %)	T_1	T_2	T_3	H_2/Zn ratio
Zn/ZSM-5(20)-IWI-(0.16)	0.8	62		520	0.17
Zn/ZSM-5(20)-IWI-(0.40)	2	60		588	0.23
Zn/ZSM-5(20)-IWI-(0.70)	3.5	60	437	640	0.30
Zn/ZSM-5(20)-CVD(DMZ)/OX-(1.00)	2.9		440	630	0.04
Zn/ZSM-5(20)-CVD(DMZ)/RED/OX-(0.41)	4.1	422	551	750	0.45

Zn/ZSM-5-IWI and Zn/ZSM-5-CVD(m), a reduction peak below 100 °C is observed, which corresponds to the H_2 uptake due to heterolytic dissociation of H_2. Previous studies[26] reported that the heterolytic dissociation of H_2 takes place at moderate temperatures and is promoted by isolated Zn^{2+} sites (reaction 4).

$$Z^-Zn^{2+}Z^- + H_2 \rightarrow Z^-Zn^{2+}{-}H^- + H^+Z^- \quad (5)$$

For the samples prepared by IWI, the total H_2/Zn ratio increases with the zinc content. In addition to the hydrogen peak below 100 °C, the Zn/ZSM-5(20)-IWI catalysts also show a reduction feature at higher temperatures that is associated with the reduction of oxygenated Zn aggregates. Its position is close to that observed for the reduction of bulk zinc oxide, which occurs around 570 °C (upper trace in Figure 1A). The low H_2 consumption observed for ZnO is caused by the low surface area of the particles, where the actual reduction takes place. The high-temperature reduction peak for the zeolitic samples is more intense because of the much smaller size of the zinc oxide-like particles confined in the micropores of ZSM-5 zeolite.

Qualitatively, the TPR profile obtained for Zn/ZSM-5(20)-CVD(m) is similar to the profiles found for the samples prepared by IWI. The pronounced low-temperature reduction peak in this case is followed by a release of H_2 in the range of 150−350 °C, evidencing the reversibility of the dissociative H_2 adsorption. Although Zn/ZSM-5(20)-CVD(m) and Zn/ZSM-5(20)-IWI-(0.70) samples consume comparable amounts of H_2 at low temperatures, the hydrogen evolution of the former material between 150 and 350 °C is much higher. This observation can be rationalized by taking into account that Zn/ZSM-5(20)-CVD(m) predominantly contains isolated Zn^{2+} ions, whereas the speciation of Zn in Zn/ZSM-5(20)-IWI-(0.70) is much more heterogeneous and may include multinuclear oxygenated clusters. These findings seem to agree with results from computational studies[40] showing that although oxygenated $[ZnOZn]^{2+}$ species and isolated Zn^{2+} sites show comparable reactivity for the heterolytic dissociation of

dx.doi.org/10.1021/cs200441e | ACS Catal. 2012, 2, 71−83

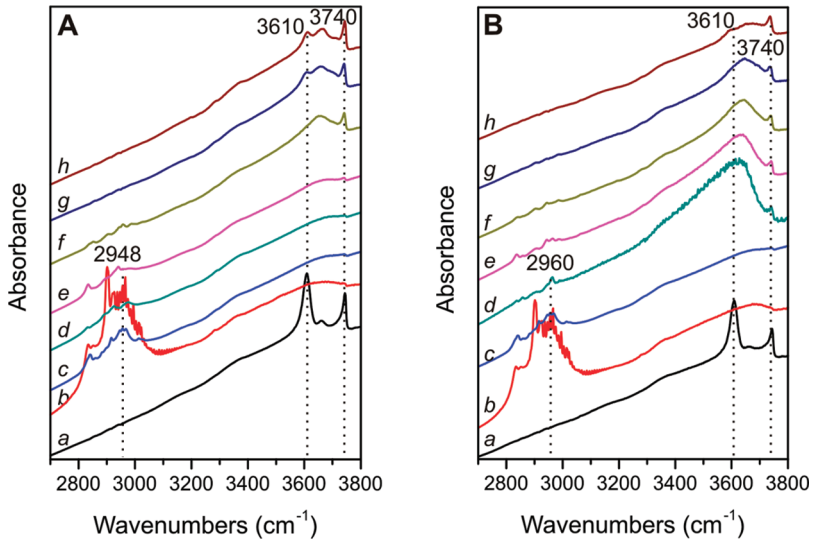

Figure 2. In situ FTIR spectra of the CVD of DMZ onto HZSM-5(20) zeolite and the decomposition of the grafted organozinc species via reduction (A) and oxidation (B). (a) Room temperature spectrum of the parent HZSM-5(20) dehydrated and evacuated at 550 °C, (b) 20 s exposure to DMZ, (c) evacuated for 20 min at room temperature, followed by reduction in H_2 (A) or O_2 (B) (50 mbar) and subsequent evacuation at (d) 100 °C, (e) 200 °C, (f) 300 °C, (g) 400 °C, (h) 500 °C.

molecular hydrogen, the reverse reaction is possible only for the mononuclear sites.

The high-temperature reduction peak in the case of Zn/ZSM-5(20)-CVD(m) is shifted to lower temperatures. This is probably due to the higher reactivity of Zn^{2+} ions at the charge-alternating sites of ZSM-5. For the Zn/ZSM-5(20)-IE samples, the TPR profiles are not informative because of the low density and low reactivity of Zn^{2+} at the exchange sites in agreement with previous studies.[4,57,58]

The TPR profile of Zn/ZSM-5(20)-CVD(DMZ) in Figure 1B also contains a low-temperature feature. In contrast to the above assignment, this H_2 consumption is most likely associated with the hydrogenolysis of the adsorbed CH_3−Zn moieties, resulting in the formation of Zn−H and release of CH_4 according to reaction 3. The reduction peak is significantly shifted to higher temperatures compared to the dissociative adsorption of H_2. A pronounced negative feature at around 360 °C and the features observed at higher temperatures (450 and 510 °C) are likely associated with the CH_4 formation. Decomposition of the grafted zinc hydride species and the release of molecular hydrogen similar to the case of Zn/ZSM-5(20)-CVD(m) can be excluded here, because this process requires the presence of a stoichiometric amount of Brønsted acid sites. The positions of these TPR features correlate very well with the maxima in methane formation detected by mass spectrometry analysis of the effluent gas (Figure 1 C).

The overall shape of the TPR profile (Figure 1B) and its relation to that of the methane evolution (Figure 1C) suggest that the features represent a superposition of a broad hydrogen consumption and the associated methane release peaks due to the hydrogenolysis of various intrazeolitic Zn-CH_3 fragments. Besides this, at higher temperatures Zn−H species are decomposed resulting in a partial reduction of Zn sites and the formation of Zn^0 contributing thus further to the complex network of chemical processes reflected in the TPR profile of the Zn/ZSM-5(20)-CVD(DMZ) zeolite. In addition, during the experiment small amounts of ethane are observed. The formation of longer hydrocarbons upon the thermal decomposition of pure DMZ has been previously reported.[59] The unsaturated hydrocarbons that were observed upon the decomposition of pure $Zn(CH_3)_2$ probably undergo hydrogenation and hydrocracking under the TPR conditions resulting in the predominant formation of methane. No traces of water are detected during the TPR experiment indicating the absence of oxygen-containing extraframework Zn species.

The decomposition of the grafted Zn-CH_3 fragments by a high-temperature treatment in O_2 atmosphere (Zn/ZSM-5(20)-CVD(DMZ)/OX-(1.00)) leads to a TPR profile that is close to that of bulk ZnO (Figure 1A). Thus, we propose that the oxidative decomposition of grafted DMZ species in ZSM-5 results in ZnO-like aggregates confined in the zeolite micropores (reaction 4). On the other hand, oxygenation of Zn ions formed by the decomposition of the grafted organozinc species in H_2 (Zn/ZSM-5(20)-CVD(DMZ)/RED/OX-(0.41)) leads to the formation of highly dispersed oxygenated cationic Zn complexes that are characterized by a reduction peak at 420 °C (Figure 1A). A similar reduction profile has been recently assigned to highly dispersed oxidic species in bimetallic dehydroaromatization ZSM-5 catalysts.[58] We propose that this low-temperature reduction feature and the rather high total H_2/Zn consumption are indicative of a high mobility of the extraframework oxygen ligands in Zn/ZSM-5(20)-CVD(DMZ)/RED/OX-(0.41). The apparent higher degree of aggregation and lower reducibility of zinc species in Zn/ZSM-5(20)-CVD(DMZ)/OX-(1.00) compared to that in the Zn/ZSM-5(20)-CVD(DMZ)/RED/OX-(0.41) sample are probably due to (i) the much higher density of zinc ions and (ii) the possibility of hydrolysis of zinc ions by water formed in situ upon the oxidation of CH_3 ligands in the former case. The lower reducibility of the larger oxygenated Zn aggregates is indicative of the decreased basicity of the extraframework O atoms shared by multiple Lewis acidic centers.[39,46]

3.3. FTIR Characterization. A rough estimation of the exchange level of Zn/ZSM-5 prepared by IE or IWI can be obtained by comparing the intensities of the OH stretching bands in the FTIR spectra (Supporting Information, Figure S2). The increase of the Zn content leads to a decrease of the intensity of the band at 3610 cm^{-1} corresponding to the

dx.doi.org/10.1021/cs200441e | ACS Catal. 2012, 2, 71−83

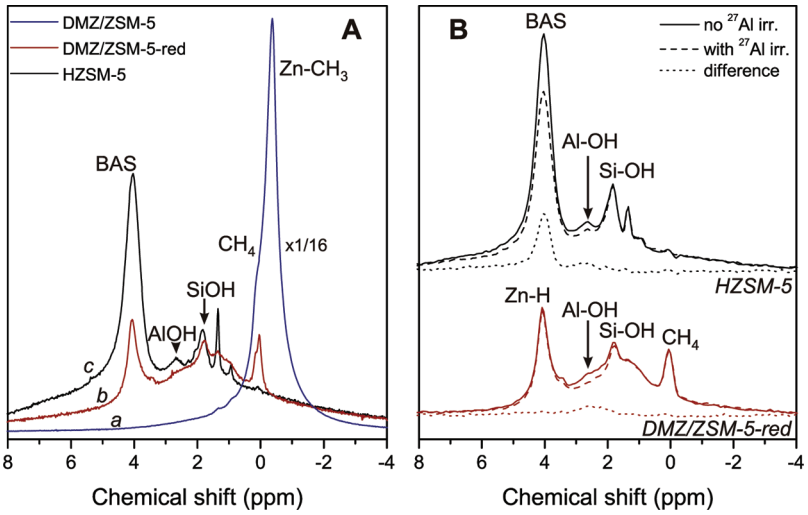

Figure 3. (A) ^{1}H MAS NMR spectra of (a) as-prepared DMZ-exposed ZSM-5 zeolite (scaled by a factor 1/16) and (b) subsequently reduced in H_2 at 300 °C. Spectrum (a) corresponds to the dehydrated parent HZSM-5(20). All samples were spun at a rate of 25 kHz in dry nitrogen gas. Panel (B) compares Hahn-echo ^{1}H NMR spectra without ^{27}Al NMR irradiation (solid lines) and ^{1}H-{^{27}Al} TRAPDOR spectra with ^{27}Al NMR irradiation (dashed lines) of the dehydrated hydrogen form (black) and the DMZ-exposed and reduced in H_2 at 300 °C Zn/ZSM-5(20) zeolite (red). The respective TRAPDOR difference spectra are given as dotted lines.

Brønsted acid sites. Even for the samples with a Zn loading above the ion-exchange capacity, the intensity of this band decreased not more than by 50% as compared to the corresponding parent HZSM-5 zeolite, evidencing only a partial exchange of the zeolitic protons by Zn cations in agreement with the above-discussed results.

The progress of the interaction of the zeolitic Brønsted acid sites with DMZ upon the CVD modification was monitored by use of in situ FTIR spectroscopy. Figure 2A shows the changes of the IR bands in the OH stretching region upon the exposure of the zeolite to DMZ and the subsequent decomposition of the grafted organometallic species in hydrogen. The introduction of DMZ at room temperature results in a complete disappearance of the bands in the hydroxyl region of the IR spectrum including those associated with Brønsted acid sites (3610 cm^{-1}), silanol groups (3740 cm^{-1}), and extraframework Al (3660 cm^{-1}). Instead, a broad absorption band appears in the region of 3300−3700 cm^{-1}. This is attributed to the physical adsorption of DMZ on the zeolitic OH groups. The adsorbed DMZ is also characterized by a set of C−H vibrations in the region 2800−3000 cm^{-1} (spectrum *b* in Figure 2A). In addition, a rotational fine-structure of the CH_3 moieties of gas-phase DMZ is observed. The latter disappears after room temperature evacuation of the sample (spectrum *c* in Figure 2A). The spectrum now contains well-resolved bands due to the C−H stretching vibrations corresponding to the DMZ adsorbed on the zeolite. After reduction in static H_2 followed by evacuation at 100 °C (spectrum *d* in Figure 2A) only two bands at 2911 and 3000 cm^{-1} corresponding to the symmetric and asymmetric C−H stretching vibrations of CH_3 groups bound to Zn are present in the IR spectrum. Upon reduction at higher temperatures, these bands disappear and some of the zeolitic OH groups are formed back (spectra *e*−*h* in Figure 2A). The silanol groups appear most easily, followed by a partial recovery of the bands from the extraframework Al (EFAL) species (3660 cm^{-1}). Only a small fraction of Brønsted acid sites (3610 cm^{-1}) is regenerated after reduction at 500 °C (Supporting Information, Figure S3).

Besides the partial regeneration of BAS, reduction at 300 and 400 °C results in the formation of zinc hydrides species characterized by a broad absorption band around 1930 cm^{-1} (see Supporting Information, Figure S3) because of the dissociative adsorption of H_2 on intrazeolitic Zn species.[26−28] The intensity of this band is approximately 3 times lower compared to that of the regenerated BAS (3610 cm^{-1}, Supporting Information, Figure S3). This is in agreement with the ratio of infrared intensities of the respective vibrations predicted by cluster density functional theory (DFT) calculations (72 and 207 km mol^{-1}, respectively for $Z^{-}Zn^{2+}H^{-}$and $H^{+}Z^{-}$ moieties).[39,60] This band disappears after the reduction/evacuation treatment at 500 °C, which at the same time results in the most pronounced partial regeneration of the zeolitic Brønsted acid sites (spectrum *h* in Figure 2A and Supporting Information, Figure S3). Thus, both the regeneration of BAS and the high-temperature reduction peak observed in the TPR experiment (Figure 1B) can be ascribed to reduction of a part of Zn^{2+} and the evaporation of Zn^{0}. This is in line with the total zinc content in the resulting Zn/ZSM-5(20)-CVD(DMZ)/RED sample (Table 1).

When the grafted DMZ species are decomposed by oxidation (spectrum *d* in Figure 2B), the formation of new broad and intense IR bands with a maximum at 3630 cm^{-1} is observed after the O_2 treatment at 100 °C. This band is probably associated with the formation of methanol, water, and/or (partially) hydroxylated Zn species in the zeolite resulting from oxidation of highly reactive CH_3 ligands. The presence of weak bands with maxima at 2960 and 2856 cm^{-1} can be attributed to the residual (partially oxidized) methyl groups at the grafted zinc sites or adsorbed methanol.[61] Further oxidation at 200−300 °C results in the decrease of the intensity of the broad band at 3630 cm^{-1}, while several new bands are formed in the region of CH stretching vibrations because of oligomeric hydrocarbon species. These bands completely disappear after the treatment in O_2 at 400 °C, whereas the broad band at 3630 cm^{-1} disappears only at 500 °C.

In contrast to the case of the decomposition of grafted DMZ with H_2, the regeneration of the zeolitic Brønsted acid sites

dx.doi.org/10.1021/cs200441e | *ACS Catal.* 2012, 2, 71−83

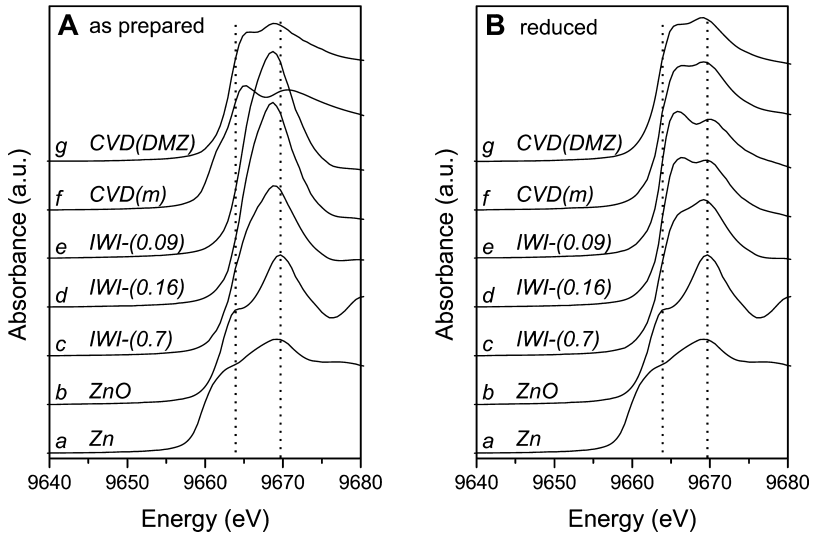

Figure 4. XANES spectra of (a) Zn foil and (b) ZnO reference materials as well as those of (A) as prepared and (B) reduced in H_2 at 550 °C Zn/ZSM-5 catalysts: (c–e) Zn-ZSM-5(20)-IWI and (f–g) Zn-ZSM-5(20)-CVD.

upon the high-temperature oxidation of the CVD(DMZ) catalyst is only minor. The Zn content in the resulting ZnZSM-5(20)-CVD(DMZ)/OX catalyst is close to unity (Table 1). This suggests that the decomposition of grafted DMZ species in oxygen leads to the formation of oxygenated multinuclear cationic Zn species compensating for the negative charge of the zeolite framework.[25]

3.4. Magic-Angle Spinning (MAS) ^{1}H NMR. The interaction of DMZ with HZSM-5(20) and its decomposition under the reductive conditions was further investigated by MAS NMR spectroscopy. Figure 3 A shows the ^{1}H MAS NMR spectra of (*a*) freshly prepared and (*b*) exposed to hydrogen at 300 °C DMZ-loaded HZSM-5 catalyst. The ^{1}H MAS NMR spectrum of dehydrated HZSM-5(20) *before* DMZ chemisorption is given for comparison (Figure 3A, spectrum *c*). The spectrum of the parent material contains signals of Brønsted acid protons (Al–OH-Si) at 4.1 ppm, hydroxyl groups connected to extra-framework aluminum (Al–OH) at 2.7 ppm, silanol moieties (Si–OH) at 1.8 ppm,[62] as well as minor alkane/alkyl signals at 1.4 and 0.9. After DMZ deposition (Figure 3A, spectrum *a*), the signals observed for the original HZSM-5(20) sample are replaced by a very large ^{1}H NMR signal at −0.4 ppm with a shoulder at 0.1 ppm corresponding, respectively, to Zn-CH_3 moieties and methane. This assignment is corroborated by the observation of corresponding ^{13}C NMR signals in the range from −16 to −13 ppm and at −9 ppm, respectively (see Supporting Information) as well as by the earlier reported ^{1}H and ^{13}C NMR shifts for Ga-CH_3 on ZSM-5 (δ_H = 0.1, δ_C −7)[63] and CH_4 on HZSM-5 ($\delta_H \sim 0$, $\delta_C \sim -11$)[64] or on Zn/H-BEA ($\delta_H \sim 0.1$, $\delta_C = -8.3$).[33]

The intensity of the Zn-CH_3 signal at −0.4 ppm in the ^{1}H MAS NMR spectrum of as-prepared DMZ-treated sample is much higher than three-times the combined intensities of the Brønsted and silanols signal at 4.1 and 1.8 ppm in the ^{1}H NMR spectrum of the parent H-ZSM-5. This indicates that the material prepared for MAS NMR measurements contains substantial amounts of unreacted physisorbed DMZ. The copresence of chemisorbed Zn-CH_3 moieties and molecularly adsorbed DMZ is consistent with the apparent distribution of ^{13}C NMR signals between −16 and −13 ppm (see Supporting Information).

After reduction of the DMZ-exposed HZSM-5 zeolite in H_2 gas at 300 °C, the −0.4-ppm signal in the ^{1}H MAS NMR spectrum has disappeared, leaving behind a small signal of residual encapsulated methane at 0.1 ppm only. At 4.1 ppm one observes what looks, at first sight, as a partly recovered Brønsted acid proton signal. However, ^{1}H-{^{27}Al} TRAPDOR, a NMR technique to distinguish between hydrogen atoms with and without Al neigbours,[55,56] shows that this ^{1}H NMR signal is much less sensitive to ^{27}Al NMR irradiation than the Brønsted acid proton signal of HZSM-5 (Figure 3). In contrast and as proven for the correct TRAPDOR experiment, the extraframework Al–OH signals at 2.7 ppm in both reduced Zn/ZSM-5(20)-CVD(DMZ) and HZSM-5 are similarly affected in this TRAPDOR experiment. The hydrogen atoms resonating at 4 ppm in the reduced DMZ-exposed HZSM-5 material thus appear to be more distant from the nearest Al atom than Brønsted acid protons from their Al neighbor. A possible explanation is the formation of zinc hydride species during the hydrogenolysis of both grafted and physically adsorbed DMZ in H_2 atmosphere. Such species may be regarded as Z^--Zn(II)H complexes with zeolite Z^- playing the role of a (solid) multidentate ligand coordinating to the zinc center via numerous available lattice basic oxygen sites. Roughly comparable organozinc hydride compounds in solution usually give a Zn-hydride signal in the range 4–5 ppm,[65,66] that is, potentially difficult to distinguish from a Brønsted acid proton signal on the basis the chemical shift alone. Zinc hydride species also act as transient reaction intermediates in alkane activation on Zn-zeolites, but such species turned out undetectable in previous NMR studies by Stepanov et al.[33−38] It should be noted, however, that the hydrogen treatment of the DMZ-exposed sample in our present study leads to the transformation of a *large* fraction of the intrazeolitic Zn into the hydride state. This is very different from the situation when Zn–H species are formed as the products of heterolytic H_2 dissociation (discussed in the previous section) or as reaction intermediates in alkane activation on highly reactive specific Zn sites.[26−30] The concentration of such reactive complexes is very low in conventional catalysts.[29] The increased concentration of intrazeolitic zinc hydride species, which are not necessarily representative of the complexes formed in the course of the

dx.doi.org/10.1021/cs200441e | *ACS Catal.* 2012, 2, 71–83

catalytic alkane dehydrogenation, explains the possibility of their detection by use of ^{1}H MAS NMR.

3.5. XAS. XAS at the Zn K-edge was used to investigate the influence of the preparation method on the nature and coordination properties of Zn species in Zn/ZSM-5. Figure 3 shows XANES spectra of Zn-ZSM-5(20)-IWI samples with different zinc loading and the catalysts prepared by the CVD methods. The respective Fourier transforms of EXAFS spectra and their fits are shown in Figure 4, while the EXAFS fit parameters are summarized in Table 3.

Table 3. EXAFS Fit Parameters of As Prepared and Reduced Zn/ZSM-5 Catalysts[a]

	backscatter	N^b	R, Å^c	$\Delta\sigma^2$, Å ^{d}	ΔE_0, eV^e
	Zn/ZSM-5(20)-IWI-(0.09)				
as prepared:	Zn−O	5.04	2.085	0.021	−3.59
	Zn−Zn	0.03	2.700	0.002	
reduced:	Zn−O	4.16	2.021	0.018	−2.50
	Zn−Zn	0.38	3.000	0.020	
	Zn/ZSM-5(20)-IWI-(0.16)				
as prepared:	Zn−O	4.82	2.081	0.022	−4.12
	Zn−Zn	0.33	2.852	0.022	
reduced:	Zn−O	3.59	1.989	0.018	−3.33
	Zn−Zn	1.17	3.199	0.009	
	Zn/ZSM-5(20)-IWI-(0.70)				
as prepared:	Zn−O	5.18	2.009	0.025	−3.33
	Zn−Zn	2.49	3.220	0.020	
reduced:	Zn−O	4.77	1.993	0.024	−3.33
	Zn−Zn	1.32	3.209	0.016	
	Zn/ZSM-5(20)-CVD(m)				
as prepared:	Zn−O	2.72	1.965	0.018	−1.04
	Zn−Zn	0.13	2.912	0.001	
reduced:	Zn−O	4.41	1.993	0.022	−1.13
	Zn−Zn				
	Zn/ZSM-5(20)-CVD(DMZ)				
as prepared:	Zn−O	4.70	1.960	0.018	−2.27
	Zn−Zn	0.19	3.269	0.008	
reduced:	Zn−O	4.80	1.981	0.020	−2.27
	Zn−Zn	0.50	3.262	0.012	

[a]Coordination numbers and distances in reference materials: Zn^0 foil: N_1(Zn−Zn) = 6, r_1(Zn−Zn) = 2.665 Å, N_2(Zn−Zn) = 6, r_2(Zn−Zn) = 2.913 Å; bulk ZnO: N(Zn−O) = 4, r(Zn−O) = 1.970 Å, N(Zn−Zn) = 6, r(Zn−Zn) = 3.250 Å. [b]Coordination number (N) ± 20%. [c]Coordination distance (R) ± 0.04 Å. [d]Debye−Waller factor ($\Delta\sigma$2) ± 10%. [e]Inner potential (ΔE^0).

The position of the absorption edge in the XANES spectra depends on the oxidation state of Zn. For example, oxidation of Zn^0 to Zn^{2+} results in a substantial shift of the adsorption edge in XAS spectrum to higher energies (9659 and 9662 eV, respectively, for Zn^0 and ZnO). For all Zn/ZSM-5 samples considered here, the Zn K-edge position (9663 eV) was not influenced by the preparation method or by the postsynthetic high-temperature gas treatments. The location of the absorption edge of these samples is very close to that of bulk ZnO indicating that zinc is predominantly present as Zn^{2+} ions.

The shape of the XANES spectra for the hydrated Zn-ZSM-5(20)-IWI materials (Figure 4A(c−e)) is characteristic for six-coordinated octahedral complexes.[67,68] The increase of the Zn loading results in a more pronounced splitting of the main edge peak similar to the spectrum for bulk ZnO (Figure 4b). The corresponding EXAFS data (Figure 5A, Table 3) indicate that the first coordination shell around zinc for all impregnated catalysts in their hydrated form, contains about five oxygen atoms (Table 3). Taking into account the differences observed in the XANES spectra, the shortening of the Zn−O coordinations along with the increase of Zn loading is due to the increasing contribution from larger bulk ZnO aggregates. This is in line with the observation that for Zn/Al ratio of 0.09, only a minor Zn−Zn coordination is observed, while it increases gradually in Zn-ZSM-5(20)-IWI-(0.16) and Zn-ZSM-5(20)-IWI-(0.7) catalysts. Thus, the XAS spectra of the impregnated Zn/ZSM-5 (Figure 4A and 5A) most likely correspond to a superposition of the spectra from octahedral hydrated Zn^{2+} complexes inside the zeolite pores and some larger zinc oxide aggregates. After the high-temperature treatment in H_2, a pronounced splitting of the white line is observed for all IWI samples because of the change of Zn coordination. Such splitting is generally observed for tetrahedral and square-pyramidal Zn complexes.[67,68] Accordingly, the Zn−O coordination number decreases because of the H_2O removal. It is important to note that for the Zn-ZSM-5(20)-IWI-(0.09) and Zn-ZSM-5(20)-IWI-(0.16) catalysts the high-temperature treatment results in an increase of the Zn−Zn coordination because of the condensation of partially hydroxylated $[Zn{-}OH]^+$ species into multinuclear Zn clusters.

The XAS spectra for the catalysts prepared by CVD methods are quite different. In the case of the Zn/ZSM-5(20)-CVD(m), a distinct shoulder at lower energies in the XANES spectrum (Figure 4A(f)) suggests the presence of a considerable amount of metallic zinc in the sample that disappears upon the high-temperature treatment. The overall shape of the white line both before and after the reduction indicates that the major part of Zn is present as four- and five-coordinated complexes in line with the results of the EXAFS analysis (Figure 5A and B (d), Table 3). The relatively low number of neighbors in the first coordination sphere and a notable Zn−Zn coordination in the original sample reflects the presence of residual Zn^0, which is completely removed from the sample upon high-temperature treatment. In the case of the CVD of DMZ, the zinc species are predominantly present as four- and five-coordinated isolated zinc complexes. High-temperature reduction does not lead to notable changes in the XAS spectra (Figures 4 and 5, Table 3).

In summary, Zn/ZSM-5 catalysts prepared by IWI methodology exhibit a large degree of heterogeneity of the zinc species. At higher Zn loading, a substantial contribution from bulk ZnO is detected in the respective XAS spectra. High temperature treatment under reducing conditions has a strong effect on the state of zinc in the IWI catalysts. Even at low zinc loading a considerable aggregation of Zn species is observed. In contrast, both CVD of Zn vapor and DMZ result in a more homogeneous distribution of Zn species in the zeolite micropore space with predominant formation of isolated Zn^{2+} ions.

3.6. Catalytic Reactivity. Table 4 summarizes the results of the catalytic activity measurements for propane activation over HZSM-5 and Zn/ZSM-5 catalysts at 550 °C. The parent HZSM-5(20) and HZSM-5(40) zeolites exhibit low but stable catalytic activity. Propane conversion in these cases proceeds via protolytic cracking over the BAS and yields methane and ethylene in comparable molar amounts and propene. The conversion of propane is lower for HZSM-5(40) because of the lower density of the catalytic BAS. No higher hydrocarbons were detected in the effluent gas phase. For both zeolites the

dx.doi.org/10.1021/cs200441e | ACS Catal. 2012, 2, 71−83

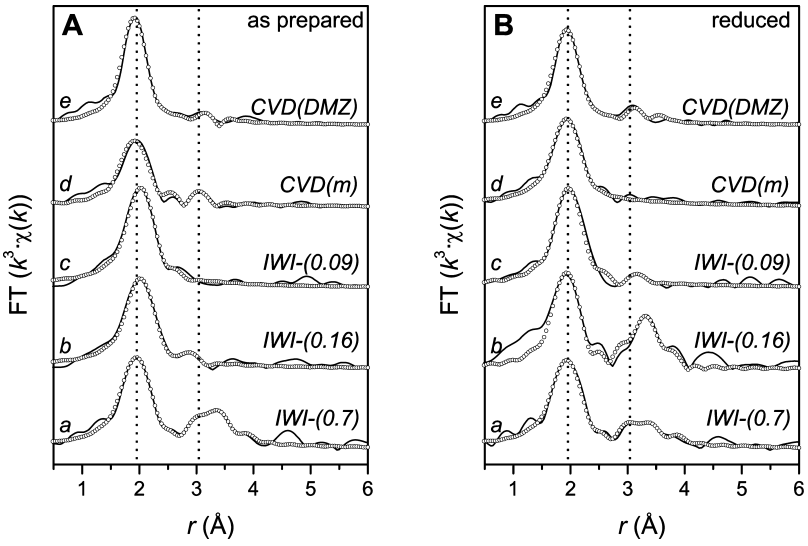

Figure 5. FTs of the EXAFS spectra of (A) as prepared and (B) reduced in H_2 at 550 °C Zn/ZSM-5 catalyst: (a−c) Zn-ZSM-5(20)-IWI and (d−e) Zn-ZSM-5(20)-CVD.

Table 4. Activity and Selectivity of Zn-Modified ZSM-5 Catalysts in Propane Cracking/Dehydrogenation[a]

			selectivity, %							
	conversion,%		initial				end			
sample	initial	end	C1	C2	C3	BTX	C1	C2	C3	BTX
HZSM-5(20)	4	4	40	44	16	0	38	42	20	0
HZSM-5(40)	2	1	43	45	12	0	46	43	11	0
Zn/ZSM-5(20)-IWI-(0.09)	8	8	14	16	67	3	15	17	66	2
Zn/ZSM-5(20)-IWI-(0.16)	34	14	11	17	60	12	12	12	73	3
Zn/ZSM-5(20)-IWI-(0.40)	34	11	11	16	61	12	12	11	74	3
Zn/ZSM-5(20)-IWI-(0.70)	50	8	15	24	42	19	11	10	77	2
Zn/ZSM-5(40)-IWI-(0.11)	6	6	20	16	64	0	20	16	64	0
Zn/ZSM-5(40)-IWI-(0.26)	18	13	11	18	64	7	11	15	71	3
Zn/ZSM-5(40)-IWI-(0.38)	16	12	10	15	65	10	11	14	72	3
Zn/ZSM-5(40)-IWI-(1.01)	30	15	14	21	52	13	12	14	70	4
Zn/ZSM-5(20)-IE(1 h)-(0.07)	7	9	18	20	61	1	15	17	66	2
Zn/ZSM-5(20)-IE(4 h)-(0.10)	12	10	13	15	69	3	14	16	67	3
Zn/ZSM-5(20)-IE(16 h)-(0.17)	29	12	10	14	69	7	10	13	73	3
Zn/ZSM-5(20)-CVD(m)-(0.57)	20	14	10	14	69	6	10	13	73	4
Zn/ZSM-5(20)-CVD(DMZ)/RED-(0.41)	27	12	11	17	61	11	9	13	75	3
Zn/ZSM-5(20)-CVD(DMZ)/RED/OX-(0.41)	42	17	11	17	62	10	9	11	79	1
Zn/ZSM-5(20)-CVD(DMZ)/OX-(1.00)	36	13	16	22	48	14	13	14	69	4

[a]50 mg catalyst, atmospheric pressure, T = 823 K, WHSV = 11.8 h^{-1} (WHSV = weight-hourly space velocity); [C_1] methane; [C_2] ethylene; [C_3] propylene; [BTX] benzene, toluene, xylenes.

conversion and the product composition remained nearly constant during the reaction.

The introduction of zinc changes the catalytic behavior of the catalysts (Table 4). The initial propane conversion is much higher for all Zn/ZSM-5 zeolites compared to the parent materials and increases with the Zn content. The methane selectivity of these Zn-containing catalysts is much lower than for the protonic zeolites, indicative of the lower BAS density. For the IWI and IE catalysts with comparable Zn content the catalytic reactivity is similar. At the initial stage of the catalytic reaction, propylene is the main product, whereas only small amounts of ethylene and methane are formed. The differences in the product composition for Zn/ZSM-5 and HZSM-5 catalysts result from the different mechanism of alkane activation by the Lewis acidic zinc and zeolitic BAS. In addition to short-chain hydrocarbons the formation of aromatic products is also detected. The highest BTX (benzene, toluene, xylenes) selectivity is observed for the most active samples prepared by IWI and having the highest Zn loading. For the Zn/ZSM-5-IE family of catalysts the BTX selectivities are lower. These catalysts also deactivate strongly during the reaction. After 4 h time on stream, all IWI and IE Zn/ZSM-5 catalysts show a stable conversion of 8−14%. The deactivation of the zeolite catalysts also leads to a lower aromatics yield.

The higher aromatization activity of the Zn/ZSM-5-IWI samples with higher Zn content is due to the presence of multinuclear oxygenated Zn species or a higher concentration of BAS. The synergetic role of both of these sites for the aromatization activity of Zn-loaded zeolites has recently been proposed by Stepanov et al.[33,35−38] Similarly, the selectivity changes observed during the deactivation can be ascribed to the decomposition of the oxygenated zinc aggregates in the

dx.doi.org/10.1021/cs200441e | ACS Catal. 2012, 2, 71−83

Table 5. Effect of Water Co-Feeding on the Catalytic Activity[a] of Zn/ZSM-5(20)-CVD(DMZ)/RED Catalyst in Propane Activation

			selectivity, %							
	conversion,%		initial				end			
pressure (kPa)	initial	1 h	C1	C2	C3	BTX	C1	C2	C3	BTX
0.00	27	24	11	17	61	11	10	16	65	9
0.05	38	35	10	13	60	17	10	14	65	11
0.10	44	35	9	13	47	31	9	11	59	21
0.50	27	25	14	12	63	11	13	11	67	9
1.00	33	27	15	10	60	15	14	10	65	11

[a]50 mg catalyst, atmospheric pressure, T = 823 K, WHSV = 11.8 h^{-1} (WHSV = weight-hourly space velocity); [C_1] methane; [C_2] ethylene; [C_3] propylene; [BTX] benzene, toluene, xylenes.

reducing atmosphere or to the deactivation of the acidic protons because of the coke formation.[2]

Although the Zn/ZSM-5(20)-CVD(m) catalyst prepared by a high-temperature reaction with zinc vapor contains the highest amount of homogeneously distributed isolated Zn^{2+} cations, its activity is close to the catalytic performance of the IWI and IE samples. This suggests that only a part of isolated Zn^{2+} ions contributes to the dehydrogenation activity of Zn/ZSM-5. Somewhat lower aromatization selectivity is observed in this case supporting the importance of residual Brønsted acid sites for the oligomerization and cyclization reactions of olefins. Product selectivities change only slightly upon catalyst deactivation. Deactivation in this case is probably associated with coke formation on the zeolitic protons upon alkene reactions or on the Zn species themselves via a mechanism similar to that recently postulated for extraframework Ga cations.[69]

The Zn/ZSM-5(20)-CVD(DMZ)/RED catalyst exhibits a somewhat higher reactivity compared to Zn/ZSM-5(20)-CVD(m). Taking into account that the selectivity toward the cracking products are similar for both catalysts, the higher initial conversion of propane and the somewhat enhanced selectivity toward aromatics are due to the synergetic effect between the extraframework zinc species and neighboring Brønsted acid sites formed during the high-temperature reduction in H_2.

A substantially higher propane conversion is observed when the reduced catalyst is oxidized prior to the catalytic experiment (Zn/ZSM-5(20)-CVD(DMZ)/RED/OX-(0.41)). We assign such an enhancement of the catalytic activity to the formation of oxygenated zinc complexes. The basicity of extraframework oxygen anions in small oxidic clusters is higher than the oxygen anions of the zeolite framework.[39,46] As a result, the initial activation of propane proceeds with lower barrier over such sites. It is likely that these extraframework clusters have a low nuclearity such as frequently proposed $[ZnOZn]^{2+}$ [10,11,17,25,39] or more recently suggested $[ZnO_2Zn]^{2+}$ [70] binuclear oxygen-bridged cationic complexes. When the same precursor is directly activated in an oxidizing atmosphere without reductive pretreatment, Zn/ZSM-5(20)-CVD(DMZ)/OX-(1.00) shows lower reactivity than Zn/ZSM-5(20)-CVD(DMZ)/RED/OX-(0.41). It is thus likely that the direct oxidative treatment of grafted DMZ species leads to the formation of oxygenated zinc aggregates with a higher than two nuclearity or even bulk-like ZnO aggregates. The difference with the sample obtained by oxidation following prereduction is most likely due to the higher density and higher reactivity of the initial Zn complexes in the Zn/ZSM-5(20)-CVD(DMZ)-(1.06) compared to Zn/ZSM-5(20)-CVD(DMZ)/RED-(0.41). The larger ZnO aggregates can be expected to be less active for propane activation, because the extraframework oxygen ligands in this case are less basic due the presence of more Zn neighbors than in binuclear cationic Zn complexes.

The initial activation of CH bonds over an extraframework Zn−O Lewis acid−base pair results in the formation of an OH group bound to Zn. To close the catalytic cycle, the regeneration of the oxygenated site proceeds via release of an H_2 molecule by recombination of a proton from the OH group with a hydride from a β-CH from the surface alkyl intermediates or a Zn−H moiety.[39] The favorability of this elementary step is controlled to a large extent by the acidity of the OH group. In dispersed oxygenated Zn species, the extraframework OH ligand bound to Zn is rather basic. Thus, the dissociation of the O−H bond required for the H_2 formation is expected to be much less favorable compared to the dissociation of the Zn−OH bond leading to the reduction of the active complex via water elimination. A similar understanding has been reported earlier for Ga/ZSM-5 zeolites.[46]

It may thus be argued that the deactivation of the oxidized Zn/ZSM-5 is in part caused by decomposition of the reactive oxygenated clusters.[2] Obviously, it is not possible to stabilize the activity by addition of molecular oxygen because it would lead to oxidation of the intermediate olefins. Another approach is to oxidize isolated Zn^{2+} ions in situ by water in a similar manner as explored before for Ga/ZSM-5 catalysts.[46] We tentatively propose that at a high temperature the interaction of extraframework cations with water will lead to their partial hydrolysis. The subsequent condensation and/or dehydrogenation of the formed hydroxylated species effectively results in the regeneration of the reactive oxygenated zinc species.

Table 5 shows the results of catalytic activity measurements of the addition of water to the feed mixture for reduced Zn/ZSM-5(20)-CVD(DMZ)/RED. It can be clearly seen that water cofeeding strongly increases propane conversion and a maximum is observed at a water partial pressure of 0.1 kPa. This maximum activity is similar to that of Zn/ZSM-5(20)-CVD(DMZ)/RED/OX-(0.41). The main products of the reaction are propylene and aromatics and at least up to a water partial pressure of 0.1 kPa the methane selectivity remains constant, suggesting that no significant amount of BAS are formed because of hydrolysis and extensive aggregating of Zn. Given the increase of methane selectivity upon a further increase of the water content in the feed, it appears that the latter does happen under such conditions. This further underpins our conclusion that especially highly dispersed multinuclear cationic Zn complexes are very active for propane

dx.doi.org/10.1021/cs200441e | ACS Catal. 2012, 2, 71−83

activation and not so much the more agglomerated forms of Zn. It is thus particularly important to stabilize oxygenated Zn clusters of high dispersion. An increase of the density of BAS associated with further agglomeration of such clusters because of an increase of the water partial pressure is not beneficial. Indeed, whereas in the case of the preoxidized Zn/ZSM-5(20)-CVD(DMZ)/RED/OX catalyst propane conversion after 1 h decreased to 19%, it remained well above 30% upon water cofeeding (Table 5).

4. CONCLUSIONS

A ZSM-5 zeolite with a homogeneous dispersion of Zn cations can be prepared by reacting HZSM-5 with the organometallic dimethylzinc precursor at room temperature. The methyl ligands of the $[ZnCH_3]^+$ ions can be removed by reduction in hydrogen, resulting in isolated Zn^{2+} stabilized at cation-exchange sites. Part of the Zn is removed upon the high-temperature reduction leading to a final Zn/Al ratio of 0.41, close to the value obtained by the CVD of HZSM-5 with Zn vapor. Unlike conventional impregnation and ion-exhange methods that result in various Zn species, the organometallic route leads to isolated extraframework $[Zn\text{-}CH_3]^+$ ions. By changing the conditions of high-temperature decomposition of this precursor, the properties of the catalytically active zinc complexes in the thus prepared Zn/ZSM-5 materials can be varied. For example, while reduction leads to the predominant formation of isolated Zn^{2+} ions, high-temperature oxidation treatment results in oxygenated cationic Zn complexes.

The catalytic behavior of Zn/ZSM-5 during propane conversion is different from that of the Brønsted acid sites in HZSM-5. Whereas protolytic cracking dominates in HZSM-5, the presence of zinc leads to strong enhancement of the rate of propane dehydrogenation. The activity of IWI and IE prepared Zn/ZSM-5 generally increases with Zn content. Although Zn/ZSM-5(20)-CVD(m) contains predominantly homogeneously dispersed isolated Zn cations, its performance is substantially lower than that of the IWI catalysts containing comparable amounts of Zn. Thus, clustered oxygenated zinc species are more active than isolated sites.

The initial catalytic activity and the product distribution of reduced Zn/ZSM-5-CVD(DMZ) is comparable to other conventionally prepared catalysts containing predominantly isolated Zn^{2+} cations. Oxidation of reduced Zn/ZSM-5-CVD(DMZ) results initially in a 2-fold increase of the propane conversion, while the product distribution remains unchanged. This activity enhancement is ascribed to the formation of more active highly dispersed oxygenated zinc complexes. The higher activity of such oxygenated species results from the higher basicity of the extraframework oxygen species and therefore to more facile initial CH bond activation. These sites, however, decompose in the course of the reaction via water desorption to the more stable isolated Zn^{2+} sites. When larger oxygen-containing Zn aggregates are formed by the direct oxygenation of the DMZ-exposed catalyst, the propane dehydrogenation activity is lower. The highly dispersed multinuclear cationic Zn complexes thus exhibit a much higher activity toward propane activation than the more agglomerated forms of Zn.

A substantial steady-state concentration of such dispersed oxygenated Zn clusters in Zn/ZSM-5 can be achieved by addition of steam to the hydrocarbon feed, leading to increased catalyst activity and stability. When higher water concentrations are cofed, activity decreases as a result of the hydrolysis of the extraframework cationic Zn complexes to less active aggregated Zn clusters.

■ ASSOCIATED CONTENT

Ⓢ Supporting Information

Supplementary TPR, FTIR, and ^{13}C MAS NMR results for Zn/ZSM-5 catalysts; in situ FTIR monitoring of the CVD of DMZ onto SiO_2 material. This material is available free of charge via the Internet at http://pubs.acs.org.

■ AUTHOR INFORMATION

Corresponding Author

*Phone: +31-40-247-2189. E-mail: e.a.pidko@tue.nl.

■ ACKNOWLEDGMENTS

DUBBLE and its staff of The Netherlands Organization for Scientific Research (NWO) are acknowledged for access to X-ray absorption facilities at ESRF Grenoble.

■ REFERENCES

(1) Ono, Y. *Catal. Rev. Sci. Eng.* **1992**, *34*, 179.
(2) Hagen, A.; Roessner, F. *Catal. Rev. Sci. Eng.* **2000**, *42*, 403.
(3) Biscardi, J. A.; Iglesia, E. *J. Catal.* **1999**, *182*, 117.
(4) Biscardi, J .A.; Meitzner, G. D.; Iglesia, E. *J. Catal.* **1998**, *179*, 192.
(5) Guisnet, M.; Gnep, N. S.; Alario, F. *Appl. Catal., A* **1992**, *89*, 1.
(6) Biscardi, J. A.; Iglesia, E. *Catal. Today* **1996**, *31*, 207.
(7) Biscardi, J. A.; Iglesia, E. *Phys. Chem. Chem. Phys.* **1999**, *1*, 5753.
(8) Lapidus, A. L.; Dergachev, A. A.; Kostina, V. A.; Mishin, I. V. *Russ. Chem. Bull., Int. Ed.* **2003**, *52*, 1094.
(9) Kazansky, V. B.; Subbotina, I. R.; Rane, N.; van Santen, R. A.; Hensen, E. J. M. *Phys. Chem. Chem. Phys.* **2005**, *7*, 3088.
(10) Barbosa, L. A. M. M.; van Santen, R. A. *Catal. Lett.* **1999**, *63*, 97.
(11) Yakovlev, A. L.; Shubin, A. A.; Zhidomirov, G. M.; van Santen, R. A. *Catal. Lett.* **2000**, *70*, 175.
(12) Frash, M. V.; van Santen, R. A. *Phys. Chem. Chem. Phys.* **2000**, *2*, 1085.
(13) Shubin, A. A.; Zhidomirov, G. M.; Yakovlev, A. L.; van Santen, R. A. *J. Phys. Chem. B* **2001**, *105*, 4928.
(14) Kachurovskaya, N. A.; Zhidomirov, G. M.; van Santen, R. A. *Res. Chem. Intermed.* **2004**, *30*, 99.
(15) Zhidomirov, G. M.; Shubin, A. A.; Kazansky, V. B.; van Santen, R. A. *Int. J. Quantum Chem.* **2004**, *100*, 489.
(16) Zhidomirov, G. M.; Shubin, A. A.; Kazansky, V. B.; van Santen, R. A. *Theor. Chem. Acc.* **2005**, *114*, 90.
(17) Barbosa, L. A. M. M.; Zhidomirov, G. M.; van Santen, R. A. *Catal. Lett.* **2001**, *77*, 55.
(18) Barbosa, L. A. M. M.; van Santen, R. A. *J. Phys. Chem. B* **2003**, *107*, 4532.
(19) Barbosa, L. A. M. M.; van Santen, R. A. *J. Phys. Chem. B* **2003**, *107*, 14342.
(20) Benco, L.; Bucko, T.; Hafner, J.; Toulhoat, H. *J. Phys. Chem. B* **2005**, *109*, 20361.
(21) Shubin, A. A.; Zhidomirov, G. M.; Kazansky, V. B.; van Santen, R. A. *Catal. Lett.* **2003**, *90*, 137.
(22) Aleksandrov, H. A.; Vayssilov, G. N.; Rösch, N. *J. Mol. Catal. A: Chem.* **2006**, *256*, 149.
(23) Klier, K. *Langmuir* **1988**, *4*, 13.
(24) Seidel, A.; Rittner, F.; Boddenberg, B. *J. Chem. Soc., Faraday Trans.* **1996**, *92*, 493.
(25) Penzien, J.; Abraham, A.; van Bokhoven, J. A.; Jentiys, A.; Muller, T. E.; Sievers, C.; Lercher, J. A. *J. Phys. Chem. B* **2004**, *108*, 4116.
(26) Kazansky, V. B.; Serykh, A. I. *Phys. Chem. Chem. Phys.* **2004**, *6*, 3760.
(27) Kazansky, V. B.; Pidko, E. A. *J. Phys. Chem. B* **2005**, *109*, 2103.
(28) Kazansky, V. B. *J. Catal.* **2003**, *216*, 192.

(29) Kolyagin, Y. G.; Ivanova, I. I.; Ordomsky, V. V.; Gedeon, A.; Pirogov, Y. A. *J. Phys. Chem. C* **2008**, *112*, 20065.
(30) Kolyagin, Yu. G.; Ivanova, I. I.; Pirogov, Yu. A. *Solid State Nucl. Magn. Reson.* **2009**, *35*, 104.
(31) Heemsoth, J.; Tegeler, E.; Roessner, F.; Hagen, A. *Microporous Mesoporous Mater.* **2001**, *46*, 185.
(32) Kazansky, V. B.; Serykh, A. I.; Pidko, E. A. *J. Catal.* **2004**, *225*, 369.
(33) Gabrienko, A. A.; Arzumanov, S. S.; Freude, D.; Stepanov, A. G. *J Phys. Chem. C* **2010**, *114*, 12681.
(34) Arzumanov, S. S.; Gabrienko, A. A.; Freude, D.; Stepanov, A. G. *Solid State Nucl. Magn. Reson.* **2009**, *35*, 113.
(35) Stepanov, A. G.; Arzumanov, S. S.; Gabrienko, A. A.; Parmon, V. N.; Ivanova, I. I.; Freude, D. *Chem. Phys. Chem.* **2008**, *9*, 2559.
(36) Stepanov, A. G.; Arzumanov, S. S.; Parmon, V. N.; Kolyagin, Yu. G.; Ivanova, I. I.; Freude, D. *Catal. Lett.* **2007**, *114*, 85.
(37) Stepanov, A. G.; Arzumanov, S. S.; Gabrienko, A. A.; Toktarev, A. V.; Parmon, V. N.; Freude, D. *J. Catal.* **2008**, *253*, 11.
(38) Gabrienko, A. A.; Arzumanov, S. S.; Toktarev, A. V.; Danilova, I. G.; Freude, D.; Stepanov, A. G. *Phys. Chem. Chem. Phys.* **2010**, *12*, 5149.
(39) Pidko, E. A.; van Santen, R. A. *J. Phys. Chem. C* **2007**, *111*, 2643.
(40) Barbosa, L. A. M. M.; van Santen, R. A. *J. Phys. Chem. C* **2007**, *111*, 8337.
(41) Ivanova, I. I.; Kolyagin, Y. G.; Ordomsky, V. V.; Asachenko, E. V.; Pasynkova, E. M.; Pirogov, Y. A. *J. Mol. Catal. A: Chem.* **2009**, *305*, 47.
(42) Kolyagin, Y. G.; Ordomsky, V. V.; Khimyak, Y. Z.; Rebrov, A. I.; Fajula, F.; Ivanova, I. I. *J. Catal.* **2006**, *238*, 122.
(43) Hensen, E. J. M.; Garcia-Sanchez, M.; Rane, N.; Magusin, P. C. M. M.; Liu, P. H.; Chao, K. J.; van Santen, R. A. *Catal. Lett.* **2005**, *101*, 79.
(44) Kazansky, V. B.; Subbotina, I. R.; Rane, N.; van Santen, R. A.; Hensen, E. J. M. *Phys. Chem. Chem. Phys.* **2005**, *7*, 3088.
(45) Rane, N.; Overweg, A. R.; Kazansky, V. B.; van Santen, R. A.; Hensen, E. J. M. *J. Catal.* **2006**, *239*, 478.
(46) Hensen, E. J. M.; Pidko, E. A.; Rane., N.; van Santen, R. A. *Angew. Chem., Int. Ed.* **2007**, *46*, 7273.
(47) Skatova, A. A.; Ignatov, S. K.; Dodonov, V. A.; Razuvaev, A. G.; Druzhkov, O. N. *Russ. Chem. Bull.* **1995**, *44*, 1832.
(48) Boiadjiev, V.; Tysoe, W. T. *Chem. Mater.* **1998**, *10*, 334.
(49) Boiadjiev, V.; Tysoe, W. T. *Chem. Mater.* **1998**, *10*, 1141.
(50) Steele, M. R.; Macdonald, P. M.; Ozin, G. A. *J. Am. Chem. Soc.* **1993**, *115*, 7285.
(51) Bowes, C. L.; Malek, A.; Ozin, G. A. *Chem. Vap. Deposition* **1996**, *3*, 97.
(52) U.S. Patent No. US 7195746 B2, 2007.
(53) Galinskii, A. A.; Galich, P. N. *React. Kinet. Catal. Lett.* **1988**, *38*, 281.
(54) U.S. Patent No. US 6084142, 2000
(55) van Eck, E. R. H.; Janssen, R.; Maas, W. E. J. R.; Veeman, W. S. *Chem. Phys. Lett.* **1990**, *174*, 428.
(56) Grey, C. P.; Vega, A. J. *J. Am. Chem. Soc.* **1995**, *117*, 8232.
(57) El-Maiki, El.-M.; van Santen, R. A.; Sachtler, W. M. H. *J. Phys. Chem. B* **1999**, *103*, 4611.
(58) Liu, B. S.; Zhang, Y.; Liu, J. F.; Tian, M.; Zhang, F. M.; Au, C. T.; Cheung, A.S.-C. *J. Phys. Chem. C* **2011**, *115*, 16954.
(59) Kuniya, Y.; Deguchi, Y.; Ichida, M. *Appl. Organomet. Chem.* **1991**, *5*, 337.
(60) Although infrared intensities are readily computed during the normal-mode analysis performed in ref 39, they were not reported in that work. Here we compare the DFT-computed infrared intensities for ν(Zn-H) and ν(O_z-H) in structure **IV** within **Zn Z_d** cluster, as defined in ref 39.
(61) Pelmenschikov, A. G.; Morosi, G.; Gamba, A.; Zecchina, A.; Bordiga, S.; Paukshtis, E. A. *J. Phys. Chem.* **1993**, *97*, 11979.
(62) Hunger, M.; Horvath, T. *J. Am. Chem. Soc.* **1996**, *118*, 12302.
(63) García-Sánchez, M.; Magusin, P. C. M. M.; Hensen, E. J. M.; Thüne, P. C.; Rozanska, X.; van Santen, R. A. *J. Catal.* **2003**, *219*, 352.
(64) Ernst, H.; Freude, D.; Mildner, T. *Chem. Phys. Lett.* **1994**, *229*, 291.
(65) Gutschank, B.; Schulz, S.; Bläser, D.; Boese, R.; Wölper, C. *Organometallics.* **2010**, *29*, 6133.
(66) Coles, M. P.; El-Hamruni, S. M.; Smith, J. D.; Hitchcock, P. B. *Angew. Chem., Int. Ed.* **2008**, *47*, 10147.
(67) Yachandra, V.; Powers, L.; Spiro, T. G. *J. Am. Chem. Soc.* **1983**, *105*, 6596.
(68) Hennig, C.; Hallmeier, K. H.; Zahn, G.; Tschwatschal, F.; Hennig, H. *Inorg. Chem.* **1999**, *38*, 38.
(69) Pidko, E. A.; Hensen, E. J. M.; van Santen, R. A. *J. Phys. Chem. C.* **2008**, *112*, 19604.
(70) Zhidomirov, G. M.; Larin, A. V.; Trubnikov, D. N.; Vercauteren, D. P. *J. Phys. Chem. C* **2009**, *113*, 8258.